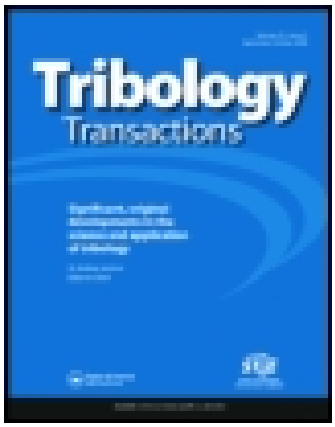

Tribology Transactions
Publication details, including instructions for authors and subscription information:
http://www.tandfonline.com/loi/utrb20

Significance of Dimple Parameters on the Friction of Sliding Surfaces Investigated by Orthogonal Experiments

Dongsheng Yan [a] , Ningsong Qu [a] , Hansong Li [a] & Xiaolei Wang [a]
[a] Nanjing University of Aeronautics & Astronautics , 29# Yudao Street, Nanjing, 210016, China
Published online: 16 Sep 2010.

To cite this article: Dongsheng Yan , Ningsong Qu , Hansong Li & Xiaolei Wang (2010) Significance of Dimple Parameters on the Friction of Sliding Surfaces Investigated by Orthogonal Experiments, Tribology Transactions, 53:5, 703-712, DOI: 10.1080/10402001003728889

To link to this article: http://dx.doi.org/10.1080/10402001003728889

Tribology Transactions, 53: 703-712, 2010

ISSN: 1040-2004 print / 1547-397X online
DOI: 10.1080/10402001003728889

STLE
Society of Tribologists and Lubrication Engineers

Significance of Dimple Parameters on the Friction of Sliding Surfaces Investigated by Orthogonal Experiments

DONGSHENG YAN, NINGSONG QU, HANSONG LI, and XIAOLEI WANG
Nanjing University of Aeronautics & Astronautics, 29# Yudao Street, Nanjing 210016, China

Surface texturing has proven to be an effective method to improve tribological performance of sliding surfaces. The pattern of microdimples is the most popular surface texture because it is supposed to obtain additional hydrodynamic pressure easily.

In order to evaluate the significance of the dimple parameters, including dimple diameter, depth, and area ratio, to the frictional performance, the dimple patterns with dimple diameter from 50 to 300 μm, dimple depth from 5 to 20 μm, and area ratio from 5 to 20% were manufactured on chromium-coated specimens by through-mask electrochemical micromachining. Experiments were designed using an L_{16} (4^5) orthogonal array, which contained the above three factors and four levels for each factor. The frictional tests on the above-textured specimens against the specimens of cast iron with oil lubrication were carried out under the contact pressures of 0.2 and 1 MPa and sliding velocities of 0.1 s and 0.5 m/s.

The range analysis showed that the optimum dimple pattern was that with dimple diameter of 100–200 μm, dimple depth of 5–10 μm, and area ratio of 5%, which induced the friction reduction up to 77.6% compared to that of untextured surfaces.

Both the range analysis and analysis of variance suggested that dimple area ratio is the most important parameter influencing friction coefficient under the test condition of this research.

KEY WORDS

Surface Texture; Orthogonal Method; Friction; Through-Mask Electrochemical Micro-Machining

INTRODUCTION

According to data from the Department of Energy of the United States summarized in 1999, reducing friction and wear in engine and drive train components could save the U.S. economy as much as US$120 billion per year (Tung and McMillan *(1)*). Energy efficiency associated with friction and wear remains an important challenge in the world's economy.

Surface texture has proven to be an effective approach to improve tribological performance of sliding surfaces. Reserving lubricant to prevent seizure is probably the earliest understanding of the lubricating mechanism of surface texture. Hence, the cross-hatch by honing has been successfully used for cylinder liners of combustion engine for more than 60 years. In the 1960s, Hamilton, et al. *(2)* proposed that micro-irregularities are able to generate additional hydrodynamic pressure to increase the load-carrying capacity of the surfaces. This theory has been well accepted, and the hydrodynamic effect is regarded as the most important effect of surface texture at the condition of high speed and low load. Based on experiments, recent research has presumed that independent and closed texture cells, such as microdimples, are better to obtain hydrodynamic effect than connected texture, such as the pattern of microgrooves (Ogihara, et al. *(3)*; Nakano, et al. *(4)*). On the other hand, as the most popular manufacturing tool, lasers are very suitable for fabricating the pattern of microdimples. Hence, surface texture of evenly distributed microdimples has attracted a lot of attention for the surface design of mechanical components.

Although advanced manufacturing techniques provide flexible and precise control of dimple geometry so the tribological performance can be further improved through the optimization of dimple shape and distribution (Nakano, et al. *(4)*; Geiger, et al. *(5)*; Kligerman, et al. *(6)*; Wang, et al. *(7)*; Costa and Hutchings *(8)*; Yu, et al. *(9)*), the pattern with the circular dimples on sliding surface is still the most popular texture pattern due to its easy fabrication and low costs.

Dimple diameter, depth, and area ratio are the major parameters of evenly distributed dimple patterns. Many researchers have contributed to the investigation of the effects of above parameters on friction or load-carrying capacity of sliding surfaces in various speed–load conditions.

Etsion's group has published analytical and experimental research papers since 1996. Their analytical models based on the Reynolds equation suggest that the preferable percentage of pore ratio is 5 to 20% (Ronen, et al. *(10)*), the optimum pore size depends on the viscosity (Etsion and Burstein *(11)*), and the effect of pore depth-over-diameter ratio is very significant (Etsion, et al. *(12)*). Their experiments show good agreement with theoretical prediction. The data on laser texturing show that the pattern of pores (ϕ90 μm, depth 2–20 μm, 25%) could increase the maximum PV value of the mechanical seal obviously (Halperin, et al. *(13)*); the pattern of pores (ϕ80 μm, depth 5.5 μm, 12%) by laser texturing could increase the maximum PV value of the mechanical seal significantly (Kovalchenko, et al. *(14)*); and with optimum

Manuscript received October 24, 2009
Manuscript accepted February 24, 2010
Review led by Farshid Sadeghi

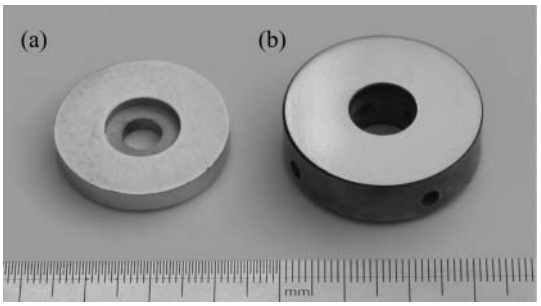

Fig. 1—Photograph of the specimens: (a) upper ring and (b) lower ring. (Figure available in color online.)

dimple depth (11 μm) and low lubricant viscosity, the texture is beneficial over the entire range of tested flow rates of lubricant for reciprocating automotive components (Ryk, et al. *(15)*). Recently, their models have been modified to suit to air bearings (Murthy, et al. *(16)*) and soft materials (Shinkarenko, et al. *(17)*).

Dumitru, et al. *(18)* investigated the effect of laser texturing in 2000. The results showed that the dimple pattern (ϕ10 μm, depth 5–8 μm, 9%) by Nd:YAG laser caused a significant increase in the lifetime of the sliding between a WC ball on an ANSI 440C steel disk.

Wang et al. introduced the surface texture for silicon carbide by both laser (Wang, et al. *(19)*) and reactive ion etching (Wang and Kato *(20)*; Wang, et al. *(21)*). The SiC disks with different dimple parameters (ϕ50–650 μm, depth 2–17 μm, 2.8–22.5%) were tested against an SiC ring under water lubrication. With sufficient water supply, there is an optimum range for depth-over-diameter ratio (0.01–0.02) and area ratio (5%), where the critical load can be improved at least twice over that of the untextured surface. However, when water was not supplied sufficiently, dimples with higher area ratio (5–15%) and deeper depth (13 μm) are preferred.

Wang and Zhu *(22)* developed a virtual texturing technique for mixed lubrication regime in 2005. The simulation results suggest that in both low-speed/high-load and high-speed/low-load conditions, the film thickness increased along with the increase of dimple diameter. In the case of low-speed/high-load, the lubrication performance is very sensitive to the variation of dimple density. For the high-speed/low-load case, there seems to be an optimal range of dimple density from 3 to 12%, where a dimple density of 5% looks to be the best choice.

Similarly, the experiments in the form of Hertzian contact carried out by Wakuda, et al. *(23)*, Pettersson and Jacobson *(24)*, Costa and Hutchings *(8)*, and Wang, et al. *(25)* showed that the dimple size might be a critical parameter for the case with high contact pressure.

As summarized above, although numerous results of the analytical and experimental works by different authors seem to be in a good correlation, the optimum values of dimple diameter, depth, and area ratio depend on the load–speed conditions, contact conditions, materials, and so on. And dimple diameter, depth, and area ratio may have different significance under different load–speed conditions.

Therefore, the aim of this article is to investigate the effect of dimple parameters on friction coefficient during sliding by experiments. The L_{16} (4^5) orthogonal array table was utilized as experimental plan for the dimple parameters including dimple diameter, depth, and area ratio. The experimental results were analyzed to evaluate the significance of these dimple parameters on the friction of sliding, and optimal values of each parameter in different load–speed conditions were suggested.

EXPERIMENT

Specimens and Surface Texturing

The friction tests were carried out between the end faces of two rings as shown in Fig. 1. The upper ring was made of ductile cast iron with chromium-plated coating about 50 μm in thickness, which has a hardness of 799 HV. The outer diameter of the upper ring was 28 mm and inner diameter was 12 mm. The lower ring was made of ductile cast iron, which has a hardness of 220 HV, outer diameter of 31 mm and inner diameter of 10 mm. The combination of these materials was adopted to simulate the friction pair of piston ring and cylinder liner of combustion engine. The surface was finished with 600# SiC abrasive paper. The end surfaces of the upper ring and lower ring had roughness *Ra* around 0.2 and 0.3 μm, respectively.

The dimple pattern was fabricated on the entire testing surface of the upper ring by photolithography and electrolytic etching techniques. The detailed process of texture fabrication is shown in Fig. 2, containing the following steps:

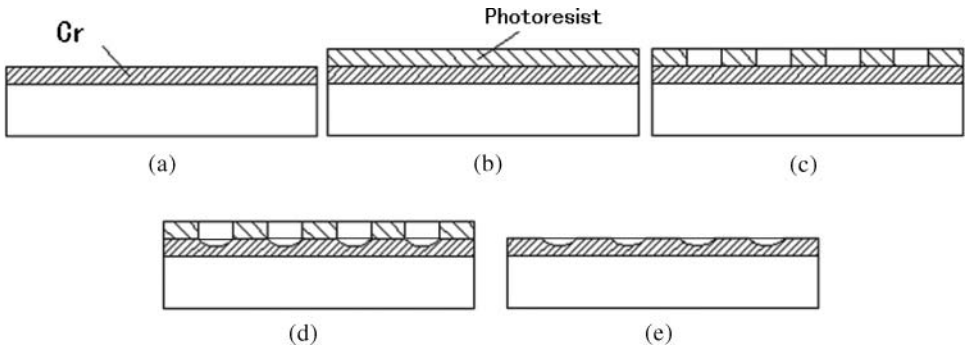

Fig. 2—Texturing process.

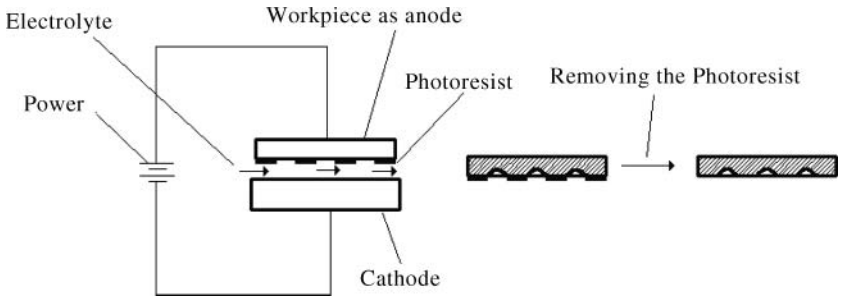

Fig. 3—Principle of electrolytic etching.

1. The surface of the upper ring was cleaned using a standard cleaning procedure.
2. A negative photoresist layer was coated on the upper ring by a spin-coater.
3. The photoresist layer was patterned with a standard lithograph process to generate a mask of photoresist.
4. The pattern was transferred to chromium film by electrolytic etching.
5. The photoresist layer was removed using solvent.

Electrolytic etching is a process to remove materials selectively by electrochemical reaction at the anode (workpiece) in an electrolytic cell as shown in Fig. 3. This method has advantages such as, regardless of material hardness, no heat affected layer, no residual stresses and cracks, etc. For the fabrication of the pattern of dimples, this method is very fast and the surface does not need to be polished again. In particular, it is easy to control the dimple diameter and depth, which is the main reason we use this method for the dimple fabrication.

Figure 4 shows the image and the profile of a dimple fabricated by photolithography and electrolytic etching techniques. The dimple diameter was around 200 μm, depth around 10 μm, and area ratio 20%. Because the side wall of the dimple was also etched during the fabrication process, the real diameter of the dimple on the surface of specimen was a little bit larger than that on the mask of photoresist. The measurements show that the real diameter of the 50 μm dimple was about 55 μm when the depth was 5 μm and 60 μm when the depth was 20 μm. For 300 μm dimple, the real diameter was about 340 μm when the depth was 20 μm. This would generate a systematic error on the testing results. The bottom of the dimple was not as flat as hoped. There were crossed microgrooves on the bottom, which usually happens on the etched chromium surface. The average depth could be controlled within $\pm$0.5 μm.

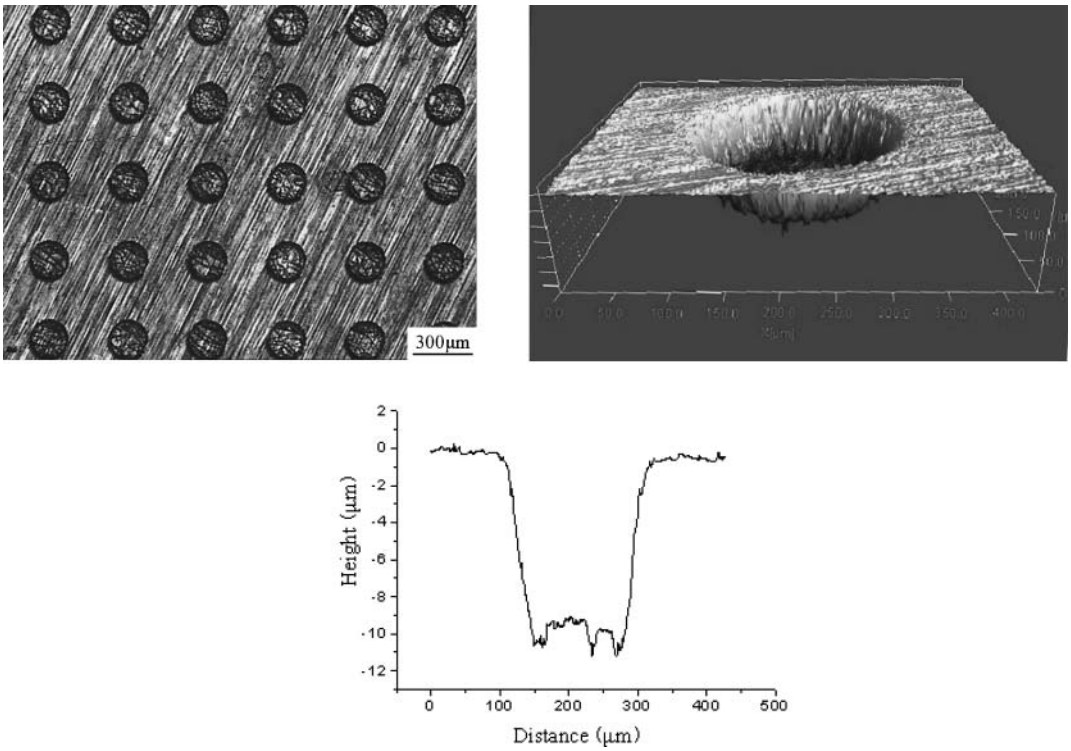

Fig. 4—Microscope image of the pattern on specimen No. 10, 3D profile and cross section of a dimple obtained by an optical profiler. (Figure available in color online.)

TABLE 1—SELECTED FACTORS OF DIMPLE PARAMETERS AND ASSIGNED LEVELS

Factor	Parameter	Unit	Level 1	2	3	4
A	Dimple diameter	μm	50	100	200	300
B	Dimple depth	μm	5	10	15	20
C	Area ratio	%	5	10	15	20

Design of Dimple Patterns

In order to investigate the effects of dimple parameters on the tribological properties efficiently, an orthogonal method was used to design the tests. Dimple diameter and depth are the main geometric parameters for a single dimple. Dimple area ratio is the parameter describing the density of the dimples distributed on the surface. These three parameters were specified as the control factors labeled as factors A, B, and C. Each factor has four levels identified by digits 1, 2, 3, and 4 as shown in Table 1. The interaction between the dimple parameters is neglected in the present study. Based on the orthogonal method, the tests were arranged using three columns of the L_{16} (4^5) orthogonal array as shown in Table 2, which contains 16 tests concerning three control factors and four levels for each factor. The advantages of this method are that each level of the control factor is repeated the same number of times (four times for this research), and the influence of each factor could be distinguished from fluctuations by statistical methods within the limited tests. The specimen marked as No. 0 represents the untextured specimen, which was added to Table 2 as a reference. Figure 5 shows the images of other specimens except No. 10, shown in Fig. 4.

TABLE 2—EXPERIMENTAL DESIGN BASED ON THE L_{16} (4^5) ORTHOGONAL ARRAY

Specimen No.	A (Dimple Diameter, μm)	B (Dimple Depth, μm)	C (Area Ratio, %)	Depth over Diameter Ratio
1	1 (50)	1 (5)	1 (5)	0.1
2	1 (50)	2 (10)	2 (10)	0.2
3	1 (50)	3 (15)	3 (15)	0.3
4	1 (50)	4 (20)	4 (20)	0.4
5	2 (100)	1 (5)	2 (10)	0.05
6	2 (100)	2 (10)	1 (5)	0.1
7	2 (100)	3 (15)	4 (20)	0.15
8	2 (100)	4 (20)	3 (15)	0.2
9	3 (200)	1 (5)	3 (15)	0.025
10	3 (200)	2 (10)	4 (20)	0.05
11	3 (200)	3 (15)	1 (5)	0.075
12	3 (200)	4 (20)	2 (10)	0.1
13	4 (300)	1 (5)	4 (20)	0.016
14	4 (300)	2 (10)	3 (15)	0.033
15	4 (300)	3 (15)	2 (10)	0.05
16	4 (300)	4 (20)	1 (5)	0.067
0	0	0	0	

Test Procedure

Friction tests were performed between the end faces of the two rings under oil lubrication at room temperature. Figure 6 shows the principle of the apparatus used in this experiment. The upper ring was mated to the lower ring and driven by a motor with a constant rotational speed. The load was applied on the lower ring by a servo motor and spring mechanism, which has a closed-loop control with a load cell for load measurement. The four holes on the side of the lower ring could help the oil flow back from the outside to the center of the ring. Friction torque was measured by a torque sensor. Frictional tests were conducted under loads of 100 and 500 N corresponding to the contact pressure of 0.2 and 1 MPa and rotational speeds of 100 and 500 rpm corresponding to the sliding speeds of 0.1 and 0.5 m/s at the average contacting radius of 10 mm.

The tests were carried out under the lubrication of an oil bath of CD15W-40 engine oil at room temperature. The process of testing is shown in Fig. 7. A large number of preliminary tests show that the friction coefficient of almost all specimens tends to be stable after running for 40 min. In order to obtain the friction coefficient in steady state, we chose the first 40 min as the process of running-in and the following 20 min as the process of testing. The friction coefficients acquired within this 20 min were averaged and used as an index to evaluate the effect of surface texture. After the running-in process for 40 min, the temperature of oil increased to 35–50°C. The viscosity η of this oil at 40°C is 115 cst.

By combining the different speeds and loads, the test conditions were set as the following four cases.

1. Low-load/low-speed (P = 0.2 MPa, V = 0.1 m/s, $\eta\omega/P = 9.58 \times 10^{-10}$);
2. Low-load/high-speed (P = 0.2 MPa, V = 0.5 m/s, $\eta\omega/P = 4.79 \times 10^{-9}$);
3. High-load/low-speed (P = 1 MPa, V = 0.1 m/s, $\eta\omega/P = 1.92 \times 10^{-10}$);
4. High-load/high-speed (P = 1 MPa, V = 0.5 m/s, $\eta\omega/P = 9.58 \times 10^{-10}$), where ω is the angular velocity in rps.

Because the untextured specimen would be the reference to be compared with other textured specimens, the test of untextured specimen was repeated eight times to acquire a more accurate result for friction coefficient. Each textured specimen was only tested once.

RESULTS AND DISCUSSION

Effect of Different Dimple Patterns on Friction Coefficient

All results of tests are shown in Fig. 8, which have the Y axis of friction coefficient μ and X axis of the number of the specimens.

Figure 8a is the case with relatively low load of 0.2 MPa and low speed of 0.1 m/s. The friction coefficient of the untextured specimen was 0.049. There were six textured specimens whose friction coefficients were decreased compared with the untextured specimen. The lowest friction coefficient was 0.024, 49% of that of the untextured specimen, obtained by specimen No. 6, which had a dimple diameter of 100 μm, depth of 10 μm, and area

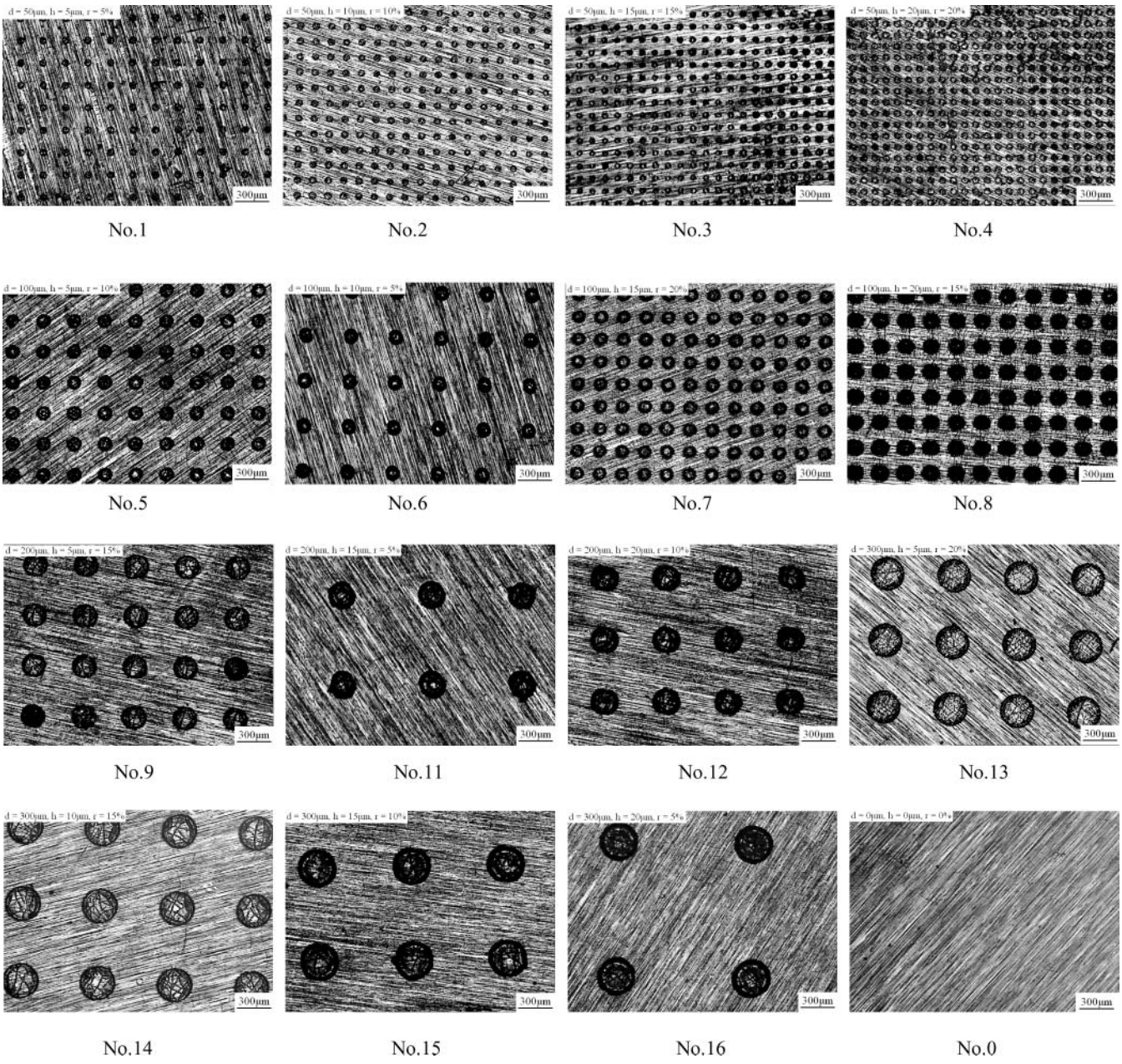

Fig. 5—Microscope images of the testing surface of upper rings.

ratio of 5%. The other specimens with relative low friction were No. 1 (ϕ50 μm, 5 μm, 5%) and No. 16 (ϕ300 μm, 20 μm, 5%).

Figure 8b is the case with relatively low load of 0.2 MPa and high speed of 0.5 m/s. By the increase of sliding speed, the friction coefficient of the untextured specimen increased to 0.080, indicating a typical mixed lubrication regime. The friction coefficients of other specimens also increased compared to that shown in Fig. 8a. Most friction coefficients of the textured specimen were lower than that of the untextured specimen. No. 6 still had low friction, but the lowest friction coefficient was obtained by No. 12, which had a dimple diameter of 200 μm, depth of 20 μm, and area ratio of 10%.

Figure 8c is the case with relatively high load of 1 MPa and low speed of 0.1 m/s. Specimen No. 6 (ϕ100 μm, 10 μm, 5%) and No. 2 (ϕ50 μm, 10 μm, 10%) presented low friction coefficient. No. 6 decreased friction about 72.8% compared to the untextured specimen.

Figure 8d is the case with relatively high load of 1 MPa and high speed of 0.5 m/s. Specimens No. 6 and No. 1 (ϕ50 μm, 5 μm, 5%), No. 2 and No. 11 (ϕ200 μm, 15 μm, 5%), and No. 16 show an obvious friction reduction effect. The maximum friction reduction rate was around 77.6%, obtained by specimen No. 6.

On the other hand, some specimens caused the friction coefficients to be higher than the untextured specimen. Specimens No.

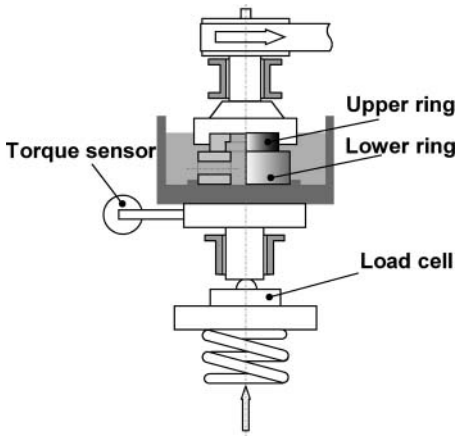

Fig. 6—Schematic diagram of the experimental apparatus. (Figure available in color online.)

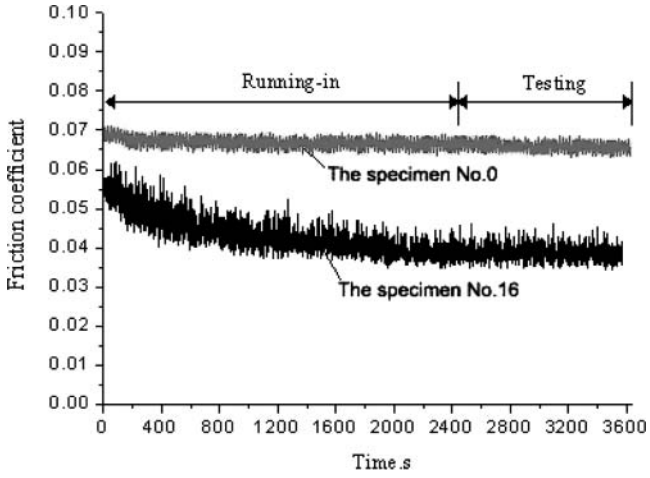

Fig. 7—The process of running-in and testing. (Figure available in color online.)

3 (ϕ50 μm, 10 μm, 15%), No. 4 (ϕ50 μm, 20 μm, 20%), No. 7 (ϕ100 μm, 15 μm, 20%), and No. 15 (ϕ300 μm, 15 μm, 10%) had a high frequency of high friction. Except for No. 15, their common feature was that their area ratio was higher than 10%.

Although there were changes in textural features that caused obvious friction reduction, it could be noticed that some levels of the parameters appeared often.

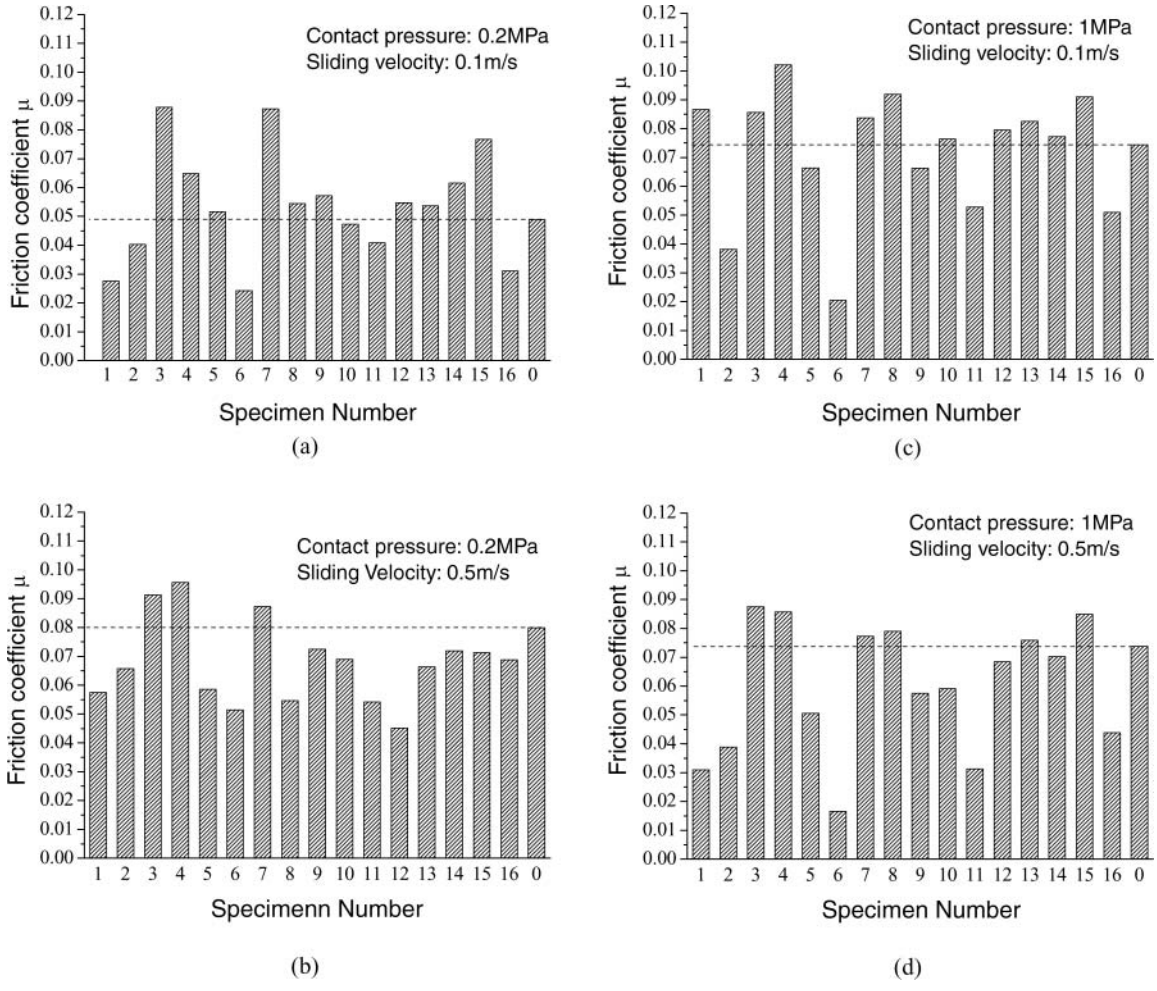

Fig. 8—Comparison of friction coefficients of the specimens at different load–speed conditions.

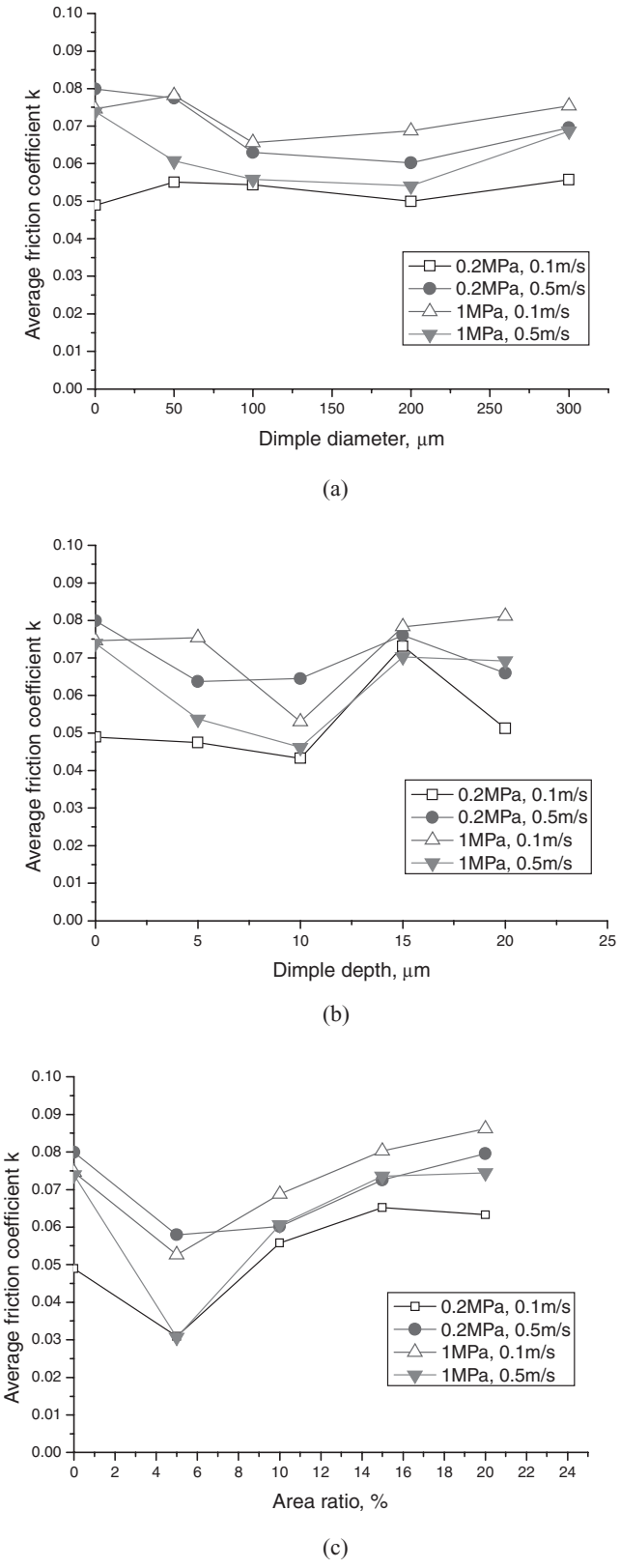

Fig. 9—Average friction coefficient as a function of different levels of (a) dimple diameter, (b) dimple depth, and (c) area ratio. (Figure available in color online.)

Effect of Dimple Parameters on Friction Coefficient Evaluated by Range Analysis

The average friction coefficients as a function of dimple diameter, depth, and area ratio are plotted in Fig. 9. The *Y* axis of the figures was drawn with the average friction coefficients at same level of corresponding factor. The *X* axis of the figures was the value of levels of each factor. For example, the square mark at the dimple diameter of 50 μm in Fig. 9a presents the average friction coefficient of specimens 1, 2, 3, and 4 at the test condition of 0.2 MPa and 0.1 m/s. These specimens have the same dimple diameter of 50 μm but different dimple depths and area ratios.

Figure 9a shows the average friction coefficient as a function of dimple diameter under different test conditions. At the condition of 0.2 MPa and 0.1 m/s, none of these average friction coefficients changed very much with an increase of dimple diameter. They were higher at diameters of 50, 100, and 300 μm, and closer but still a little bit higher at 200 μm than that of the untextured specimen. When load and speed were increased, the effects of friction reduction appeared. Particularly, for the two cases with high speed of 0.5 m/s, friction decreased obviously with the dimple diameters of 100 and 200 μm.

Figure 9b shows the average friction coefficient as a function of dimple depth under different test conditions. Except the value at the depth of 5 μm and condition of 1 MPa and 0.1 m/s, the dimple depth from 5 to 10 μm seems to be a good range in which the friction coefficient could be reduced.

Figure 9c shows the average friction coefficient as a function of dimple area ratio under different test conditions. The data for different test conditions show that the dimple area ratio from 5 to 10% was a good range, and the area ratio of 5% resulted in an obvious friction reduction.

Table 3 shows the range analysis of the L_{16} (4^5) orthogonal test results for all four test conditions. The symbol k_i represents the average friction coefficient at level i of the selected factor. For example, k_2 in column B is the average friction coefficient at level 2 of the selected factor B; that is, the average friction coefficient of the specimens that had the same dimple depth of 10 μm. The optimal level of each factor could be determined by finding the minimum k in the column of this factor. R is the difference between maximum and minimum value of the k achieved by the different levels and reflects the impact of the factor on the test results.

Based on the k value, the optimal levels of each factor at different load–speed conditions are listed in Table 3. The results show that the patterns (ϕ200 μm, 10 μm, 5%), (ϕ200 μm, 5 μm, 5%), (ϕ100 μm, 10 μm, 5%), and (ϕ200 μm, 10 μm, 5%) are the optimal for low friction at the load–speed conditions of (0.2 MPa, 0.1 m/s), (0.2 MPa, 0.5 m/s), (1 MPa, 0.1 m/s), and (1 MPa, 0.5 m/s), respectively. The values of depth-over-diameter ratio are 0.05, 0.025, 0.1, and 0.05 corresponding to each of the above cases. Not only are these values very close to those by Etsion *(12)*, but the trends agree with those by Etsion, which suggests that higher velocity or smaller clearance (by higher load) would result in smaller value of the optimal depth-over-diameter ratio.

Based on the R value, it can be found that in most cases, the influence of factors to the friction coefficient decreased in the same

TABLE 3—RANGE ANALYSIS OF THE RESULTS OF THE L_{16} (4^5) ORTHOGONAL ARRAY

Test Condition	A (Dimple Diameter)	B (Dimple Depth)	C (Area Ratio)	Influence Order
0.2 MPa 0.1 m/s				
k_1[a]	0.05508	0.04750	0.03088	C > B > A
k_2	0.05435	0.04325	0.05580	
k_3	0.04998	0.07315	0.06520	
k_4	0.05575	0.05125	0.06325	
R[b]	0.005770	0.02990	0.03432	
Optimal level	A3 (200 μm)	B2 (10 μm)	C1 (5%)	
0.2 MPa 0.5 m/s				
k_1	0.07750	0.06372	0.05800	C > A > B
k_2	0.06300	0.06450	0.06018	
k_3	0.06020	0.07600	0.07255	
k_4	0.06955	0.06600	0.07952	
R	0.01730	0.01228	0.02152	
Optimal level	A3 (200 μm)	B1 (5 μm)	C1 (5%)	
1 MPa 0.1 m/s				
k_1	0.07815	0.07542	0.05270	C > B > A
k_2	0.06562	0.05300	0.06878	
k_3	0.06878	0.07835	0.08028	
k_4	0.07538	0.08115	0.08620	
R	0.01253	0.02815	0.03350	
Optimal level	A2 (100 μm)	B2 (10 μm)	C1 (5%)	
1 MPa 0.5 m/s				
k_1	0.06075	0.05372	0.03070	C > B > A
k_2	0.05585	0.04615	0.06065	
k_3	0.05385	0.07028	0.07355	
k_4	0.06868	0.06920	0.07450	
R	0.01483	0.02413	0.04380	
Optimal level	A3 (200 μm)	B2 (10 μm)	C1 (5%)	

[a] k_i = ($\sum$ the value of selected factor at level i)/4.
[b] R = max(k_i)− min(k_i) of selected factor.

order: C > B > A. That means that the area ratio was the major factor influencing the friction coefficient. And except for the test condition of 0.2 MPa and 0.5 m/s, the secondary important factor was the dimple depth.

Significance of Dimple Parameters on Friction Coefficient by Analysis of Variance

The analysis of variance (ANOVA) could distinguish the effect of testing factor and fluctuations due to experimental error in testing results and estimate the influential degree of each factor. Therefore, the ANOVA was carried out in this research to examine the influence of dimple diameter, dimple depth, and area ratio on the friction coefficient. The results are shown in Table 4.

The fourth column of the table shows degrees of freedom (df) defined as:

$$df_j = h - 1$$

$$df_T = n - 1$$

$$df_e = df_T - df_A - df_B - df_C$$

where df_j, df_T, and df_e are degrees of freedom of factor j ($j = A$, B, C), total degrees of freedom, and degrees of freedom of error, respectively; h is the number of levels of each factor; and n is the number of total tests.

The fifth column of the ANOVA table is sum of squares (S) calculated as follows:

$$\text{The average friction coefficient } \bar{\mu} = \frac{1}{n}\sum_{i=1}^{n}\mu_i$$

$$\text{The total sum of squares } S_T = \sum_{i=1}^{n}(\mu_i - \bar{\mu})^2$$

$$\text{The sum of squares of factor } j\ S_j = \frac{n}{h}\sum_{i=1}^{h}(k_i - \bar{\mu})^2$$

$$\text{The sum of squares of error } S_e = S_T - (S_A + S_B + S_C)$$

The sixth column of the ANOVA table is mean square (MS):

$$MS_j = \frac{S_j}{df_j}$$

$$MS_e = \frac{S_e}{df_e}$$

The seventh column of the ANOVA table is F value:

$$F_j = \frac{MS_j}{MS_e}$$

F_A is the F value of factor A. Large value of F indicates that the influence of factor A on friction coefficient is more significance than that by error.

The influence degree of each factor was determined by its F ratio by the following rules:

1. If $F_j > F_{0.01}(df_j, df_e)$, the factor j is highly significant, marked as ***.
2. If $F_{0.01}(df_j, df_e) > F_j > F_{0.05}(df_j, df_e)$, the factor j is significant, marked as **.
3. If $F_{0.05}(df_j, df_e) > F_j > F_{0.1}(df_j, df_e)$, the factor j is relatively significant, marked as *.
4. If $F_j < F_{0.1}(df_j, df_e)$, the factor j is insignificant.

For the degrees of freedom $df_j = 3$ and $df_e = 6$, $F_{0.01}(3,6) = 9.78$, $F_{0.05}(3,6) = 4.76$, and $F_{0.1}(3,6) = 3.29$.

In the case of low load and low speed (0.2 MPa, 0.1 m/s), the F ratios of dimple depth and area ratio are much greater than $F_{0.01}(3,6)$, showing that both are highly significant to friction coefficient. The F ratio of area ratio is the greatest of these three factors, so area ratio is the most important factor of dimple design in this case.

Similarly, in the case of high load and high speed (1 MPa, 0.5 m/s), both area ratio and dimple depth are highly significant, and area ratio is the most important.

In the case of low load and high speed (0.2 MPa, 0.5 m/s), only the F ratio of area ratio is greater than $F_{0.1}(3,6)$, showing relatively significant for frictional performance.

In the case of high load and low speed (1 MPa, 0.1 m/s), all these three F ratios are below $F_{0.1}(3,6)$, showing that these three factors are not as significant as in other load–speed conditions conducted in this research. However, the F ratio of area ratio is still the greatest of these three factors.

Although it is still difficult to give a convincing explanation of the reasons that the influence degree of the factors changes at

TABLE 4—RESULTS OF THE ANALYSIS OF VARIANCE (ANOVA)

Test Condition	Factor	Dimple Parameter	Degrees of Freedom (d_f)	Sum of Squares (S)	Mean Square (MS)	F Ratio	Influence Degree
0.2 MPa 0.1 m/s	A	Diameter	3	0.000081	0.000027	0.58	
	B	Dimple depth	3	0.002126	0.000709	15.13	***
	C	Area ratio	3	0.002996	0.000999	21.33	***
		Error	6	0.000281	0.000047		
		Total	15	0.005484			
0.2 MPa 0.5 m/s	A	Diameter	3	0.000713	0.000238	1.95	
	B	Dimple depth	3	0.000392	0.000131	1.07	
	C	Area ratio	3	0.001257	0.000419	3.45	*
		Error	6	0.000730	0.000122		
		Total	15	0.003091			
1 MPa 0.1 m/s	A	Diameter	3	0.000402	0.000134	0.38	
	B	Dimple depth	3	0.001985	0.000662	1.88	
	C	Area ratio	3	0.002616	0.000872	2.48	
		Error	6	0.002112	0.000352		
		Total	15	0.007115			
1 MPa 0.5 m/s	A	Diameter	3	0.000510	0.000170	3.80	*
	B	Dimple depth	3	0.001684	0.000561	12.53	***
	C	Area ratio	3	0.005011	0.001670	37.30	***
		Error	6	0.000269	0.000047		
		Total	15	0.007474			

different load–speed conditions, the following several aspects of the ANOVA results are helpful for our understanding.

First of all, the F ratio of the factor of area ratio is always the greatest compared to that of the other two factors in the above four load–speed cases. Hence, there is an agreement that area ratio of the dimples plays the most important role for the performance of friction in all the load–speed conditions carried out in this research.

Secondly, the ANOVA results are similar for the cases of low load/low speed (0.2 MPa, 0.1 m/s) and high load/high speed (1 MPa, 0.5 m/s). Both area ratio and dimple depth are marked as ***. It can be noticed that the velocity-over–contact pressure ratios for these two cases are exactly the same so that their Sommerfeld numbers are also the same. That is probably why these two cases are at the same condition from the viewpoint of Stribeck curve.

Furthermore, the influence degrees of area ratio and dimple depth in the cases of low load/high speed (0.2 MPa, 0.5 m/s) and high load/low speed (1 MPa, 0.1 m/s) are not as high as the cases of low load/low speed (0.2 MPa, 0.1 m/s) and high load/high speed (1 MPa, 0.5 m/s) condition. As listed above, the Sommerfeld number ($\eta\omega$/P) of the low-load/high-speed (0.2 MPa, 0.5 m/s) condition is high, and that of high-load/low-speed (1 MPa, 0.1 m/s) is low. This might provide proof that the surface texture design needs different principles for different load–speed conditions.

CONCLUSIONS

In this study, an orthogonal method was utilized for the experimental design to evaluate the influence of dimple parameters on the frictional performance of sliding surfaces. The L_{16} (4^5) orthogonal arrays table was selected as the experimental plan, which contained three factors, including dimple diameter, dimple depth, area ratio, and four levels for each factor. The friction tests of these textured surfaces against an untextured surface were carried out under oil lubrication at four different load–speed conditions. The effects of dimple parameters on the friction coefficient were analyzed. The range analysis and analysis of variance were employed to evaluate the significance and optimal levels of these dimple parameters. The conclusions of the research are follows:

1. The results by range analysis suggest that the dimple pattern with the diameter of 100–200 μm (A2–A3), depth of 5–10 μm (B1–B2), and area ratio of 5% (C1) are the optimal for low friction at the load–speed conditions of this research. The corresponding optimal depth-over-diameter ratio is in the range 0.025–0.1 for above cases. As an example, the texture pattern with diameter of 100 μm, dimple depth of 10 μm, and area ratio of 5% has an obvious friction reduction effect, which was around 50.6% at the load–speed condition of 0.2 MPa and 0.1 m/s, 43.6% at the condition of 0.2 MPa and 0.5 m/s, 72.8% at the condition of 1 MPa and 0.1 m/s, and 77.6% at the condition of 1 MPa and 0.5 m/s, compared to the untextured surface.
2. Both the range analysis and analysis of variance suggest that dimple area ratio is the most important parameter influencing friction coefficient. The next important parameters should be dimple depth and dimple diameter at the load–speed conditions of this research. And the order of influence could change at different load–speed conditions.

ACKNOWLEDGEMENT

Financial support from the National Nature Science Foundation (NSFC, No. 50675101) and National High-tech R&D

Program (863, No. 2006AA04Z321) of China is gratefully acknowledged.

REFERENCES

(1) Tung, S. C. and McMillan, M. L. (2004), "Automotive Tribology Overview of Current Advances and Challenges for the Future," *Tribology International*, **37**, p 517.

(2) Hamilton, D. B., Walowit, J. A., and Allen, C. M. (1966), "A Theory of Lubrication by Micro-Irregularities," *Journal of Basic Engineering*, **88**, p 177.

(3) Ogihara, H., Kido, T., Yamada, H., Murata, M., and Kobayashi, S. (2000), "Technology for Reducing Engine Rubbing Resistance by Means of Surface Improvement," *HONDA R&D Technical Review*, **12**, p 93.

(4) Nakano, M., Korenaga, A., Korenaga, A., Miyake, K., Murakami, T., Ando, Y., Usami, H., and Sasaki, S. (2007), "Applying Micro-Texture to Cast Iron Surfaces to Reduce the Friction Coefficient Under Lubricated Conditions," *Tribology Letters*, **28**, p 131.

(5) Geiger, M., Roth, S., and Becker, W. (1998), "Influence of Laser-Produced Microstructures on the Tribological Behaviour of Ceramics," *Surface and Coatings Technology*, **100–101**, p 17.

(6) Kligerman, Y., Etsion, I., and Shinkarenko, A. (2005), "Improving Tribological Performance of Piston Rings by Partial Surface Texturing," *Journal of Tribology*, **127**, p 632.

(7) Wang, X. L., Adachi, K., Otsuka, K., and Kato, K. (2006), "Optimization of the Surface Texture for Silicon Carbide Sliding in Water," *Applied Surface Science*, **253**, p 1282.

(8) Costa, H. L. and Hutchings, I. M. (2007), "Hydrodynamic Lubrication of Textured Steel Surfaces under Reciprocating Sliding Conditions," *Tribology International*, **40**, p 1227.

(9) Yu, H., Wang, X., and Zhou, F. (2010) "Geometric Shape Effects of Surface Texture on the Generation of Hydrodynamic Pressure between Conformal Contacting Surfaces," *Tribology Letters*, **37**, p 123.

(10) Ronen, A., Etsion, I., and Kligerman, Y. (2001), "Friction-Reducing Surface-Texturing in Reciprocating Automotive Components," *Tribology Transactions*, **44**, p 359.

(11) Etsion, I. and Burstein, L. (1996), "A Model for Mechanical Seals with Regular Microsurface Structure," *Tribology Transactions*, **39**, p 677.

(12) Etsion, I., Kligerman, Y., and Halperin, G. (1999), "Analytical and Experimental Investigation of Laser-Textured Mechanical Seal Faces," *Tribology Transactions*, **42**, p 511.

(13) Halperin, G., Greenberg, Y., and Etsion, I. (1997), "Increasing Mechanical Seals Life with Laser-Textured Seal Faces." *15th International Conference on Fluid Sealing: BHR*, p 3.

(14) Kovalchenko, A., Ajayi, O., Erdemir, A., Fenske, G., and Etsion, I. (2005), "The Effect of Laser Surface Texturing on Transitions in Lubrication Regimes during Unidirectional Sliding Contact," *Tribology International*, **38**, p 219.

(15) Ryk, G., Kligerman, Y., and Etsion, I. (2002), "Experimental Investigation of Laser Surface Texturing for Reciprocating Automotive Components," *Tribology Transactions*, **45**, p 444.

(16) Murthy, A. N., Etsion, I., and Talke, F. E. (2007), "Analysis of Surface Textured Air Bearing Sliders with Rarefaction Effects," *Tribology Letters*, **28**, p 251.

(17) Shinkarenko, A., Kligerman, Y., and Etsion, I. (2009), "The Effect of Surface Texturing in Soft Elasto-Hydrodynamic Lubrication," *Tribology International*, **42**, p 284.

(18) Dumitru, G., Romano, V., Weber, H. P., Haefke, H., Gerbig, Y., and Pfluger, E. (2000), "Laser Microstructuring of Steel Surfaces for Tribological Applications," *Applied Physics A: Materials Science & Processing*, **70**, p 485.

(19) Wang, X., Kato, K., Adachi, K., and Aizawa, K. (2001), "The Effect of Laser Texturing of SiC Surface on the Critical Load for the Transition of Water Lubrication Mode from Hydrodynamic to Mixed," *Tribology International*, **34**, p 703.

(20) Wang, X. and Kato, K. (2003), "Improving the Anti-Seizure Ability of SiC Seal in Water with RIE Texturing," *Tribology Letters*, **14**, p 275.

(21) Wang, X., Kato, K., Adachi, K., and Aizawa, K. (2003), "Loads Carrying Capacity Map for the Surface Texture Design of SiC Thrust Bearing Sliding in Water," *Tribology International*, **36**, p 189.

(22) Wang, Q. J. and Zhu, D. (2005), "Virtual Texturing: Modeling the Performance of Lubricated Contacts of Engineered Surfaces," *Journal of Tribology - Transactions of the ASME*, **127**, p 722.

(23) Wakuda, M., Yamauchi, Y., Kanzaki, S., and Yasuda, Y. (2003), "Effect of Surface Texturing on Friction Reduction between Ceramic and Steel Materials under Lubricated Sliding Contact," *Wear*, **254**, p 356.

(24) Pettersson, U. and Jacobson, S. (2004), "Friction and Wear Properties of Micro Textured DLC Coated Surfaces in Boundary Lubricated Sliding," *Tribology Letters*, **17**, p 553.

(25) Wang, X., Liu, W., Zhou, F., and Zhu, D. (2009), "Preliminary Investigation of the Effect of Dimple Size on Friction in Line Contacts," *Tribology International*, **42**, p 1118.